Chapter 7

Physics of Strong Interactions

7.1 QCD and jet physics

7.1.1 Introduction

With the start-up of LHC, a new domain of energy will be explored and an extrapolation of our current knowledge in the form of the Standard Model may not be sufficient to describe the new measurements. Even in a first data-taking phase with a rather low luminosity, studies of jet physics in the framework of quantum chromodynamics (QCD) will allow to check our current theory against the new data.

Figure 7.1 presents the decomposition of the total jet cross section into the partonic processes for $p\bar{p}$ collisions at the Tevatron and pp collisions at the LHC in dependence of the scaling variable $x_T = 2p_{\mathrm{T}}/\sqrt{s}$, and illustrates the differences in cross section contributions of the PDFs compared to measurements possible today. In Figure 7.2 the expected statistical uncertainties on differential cross sections for all rapidities are presented for a pilot run with $0.1\,\mathrm{fb}^{-1}$ and for a first physics run with $10\,\mathrm{fb}^{-1}$. Trigger pre-scales are taken into account. The figure demonstrates that already in the pilot run high statistics will be available up to 1.5 TeV of transverse jet energy.

On the one hand, the measured data have to be corrected for detector effects using fully simulated events. Also, an energy calibration has to be performed on the reconstructed jets which ideally is extracted from data as well, but can also be done employing Monte-Carlo methods. On the other hand, for the theory predictions, which are most precise with respect to the hard parton-parton scattering amplitudes, effects of soft physics modelled in the form of parton showers and hadronisation models with subsequent decays have to be taken into account. Once this is done, parameters of the current theory can be cross-checked or improved in precision by comparing the measured hadronic final state with the corrected theoretical predictions.

7.1.2 Jet algorithms

In order to re-establish a link between the observed particles that appear as collimated streams of hadrons in the detector and the hard process, algorithms are defined to group particles that are supposed to come from the same hard parton into jets. The required ingredients of such a jet algorithm are a distance measure to define the separation between objects, a procedure how to decide when objects are to be combined and a recombination scheme explaining how to combine objects. In addition, it has to be specified how the list of input objects has been determined.

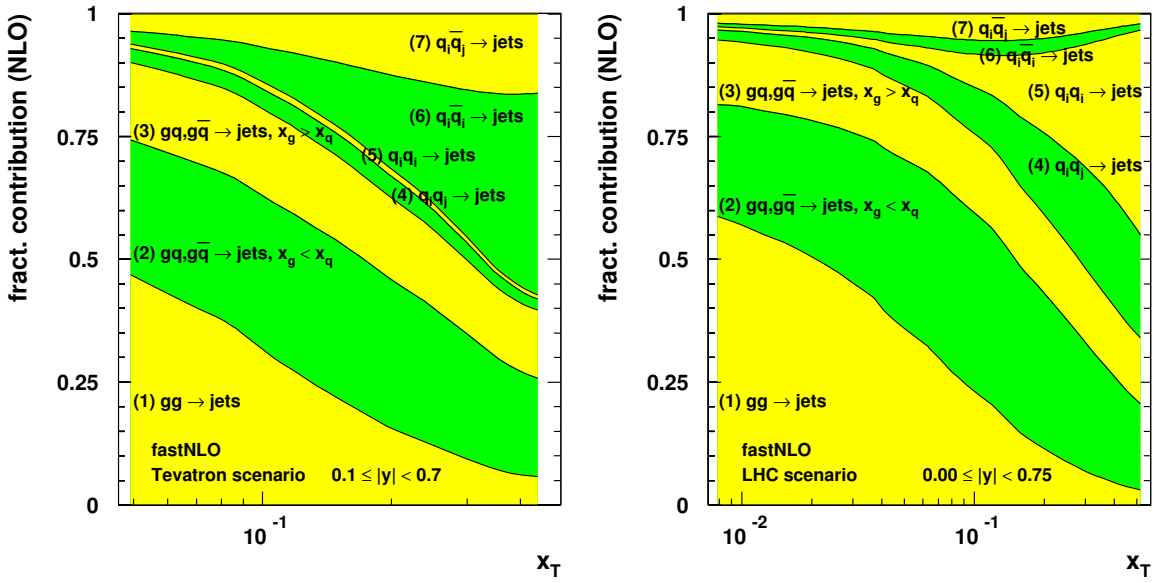

Figure 7.1: Decomposition of the total jet cross section into the partonic processes for $p\bar{p}$ collisions at the Tevatron (left) and pp collisions at the LHC (right). The fractional contributions are shown versus the scaling variable $x_T = 2p_T/\sqrt{s}$.

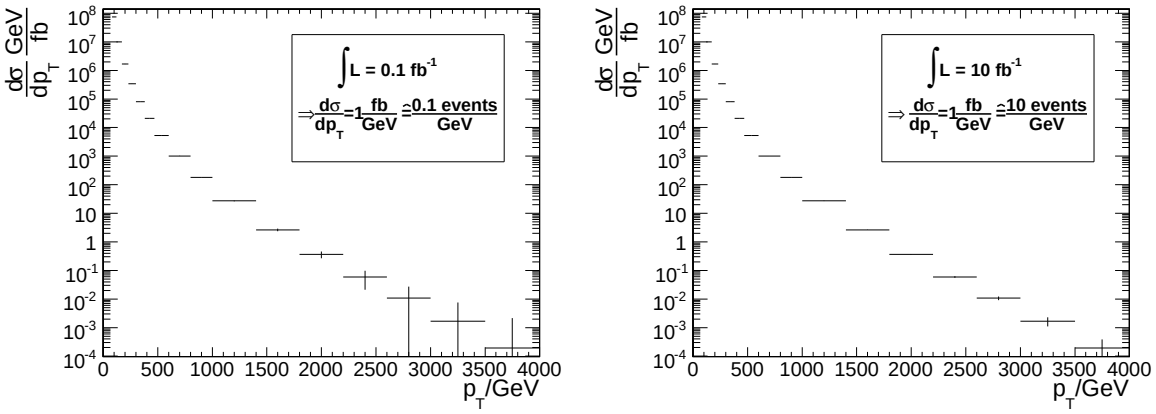

Figure 7.2: Expected statistical uncertainties on differential cross sections for all rapidities; left: for a pilot run with 0.1 fb^{-1}, and right: for a physics run with 10 fb^{-1}. The central cross section values are taken from a leading-order calculation in dependence of the transverse momenta of the hard interaction.

Two principal types of algorithms are in common use: Cone type algorithms [173] that traditionally have been employed in hadron-hadron collisions where objects are clustered together that are close in angle around a high-energetic seed, and clustering algorithms where iteratively objects are combined that have the smallest distance of all pairwise combinations possible. The latter have predominantly been used in e^+e^- and $e^\pm p$ collisions, first in the form of the Jade algorithm [174, 175] and nowadays as k_T algorithm [176].

Both algorithms applied in this study use an angular distance measure based on the azimuthal angle Φ and, instead of the pseudo-rapidity η, the true rapidity $y = 0.5\ln((E + p_z)/(E - p_z))$ which has become an established standard in recent publications [177, 178].

The distance between two objects i and j hence reads

$$\Delta R_{ij} = \sqrt{(\Delta_{ij}\Phi)^2 + (\Delta_{ij}y)^2}. \tag{7.1}$$

In addition, the most frequently used recombination scheme, the E scheme, implying a simple four-momentum addition, is employed in both cases.

Two types of jet algorithms are used here. The main results have been achieved with the k_{T} algorithm defined below, some cross checks have been performed with the midpoint cone algorithm:

1. Iterative clustering-type: Inclusive k_{T} algorithm [179] with
   - Distances are evaluated according to the ΔR scheme, i.e. $d_{ij} = \min(p_{T,i}^2, p_{T,j}^2)\frac{\Delta R_{ij}^2}{D^2}$ with R_{ij} as in eq. 7.1
   - Jet resolution parameter $D = 1.0$
2. Cone-type: Midpoint cone algorithm [180, 181] with:
   - Cone radius $R = 0.7$, all objects within a cone have to fulfill $R_{ic} \leq R$ with c labelling the four-vector of the current cone.
   - Overlap threshold $f_{\mathrm{merge}} = 0.50$, i.e. overlapping cone jets are merged when they share more than 50% of the energy in the less energetic cone
   - Search-cone radius fraction $f_{\mathrm{search}} = 0.5$, i.e. the first step to find the stable cones (before any splitting/merging is done) is performed with a smaller radius of $f_{\mathrm{search}} * R$

Concerning the k_{T} algorithm, a jet resolution parameter of $D = 1.0$ is, from a theoretical point of view, best comparable to a cone algorithm with $R = 0.7$. In order to reduce the sensitivity to the underlying event it is advantageous to reduce the jet resolution parameter D or the cone radius R, respectively.

Note that primarily due to the limited choice of available jet energy calibrations the definition of the midpoint algorithm above has been selected. It does not exactly correspond to the definition given in [180] but to a modified one [181] that is in use by the CDF collaboration [177]. There have been indications that this algorithm leads to an infrared sensitive behaviour [182], so it is recommended to use the original definition of the midpoint algorithm without extra search cone radius.

7.1.3 Trigger scheme, event selection and phase space

The level one (L1) and the high level triggers (HLT) required for this analysis are the single-jet triggers which are described in more detail in section E.4.3.2. QCD jet production has, by several orders of magnitude, the largest cross section, but in contrast to most other analyses QCD jet events are the signal here. Therefore the sole other selection requirement for this study demands all jets to have a transverse momentum larger than $50\,\mathrm{GeV}$. The available phase space is then subdivided into 17 ranges in transverse momentum p_{T} and five ranges in rapidity y, where the focus is mostly on the central region up to 2.5 in rapidity.

7.1.4 Input data

The analysed events were generated with PYTHIA [183] and subsequently subjected to the full GEANT-4 based CMS detector simulation and reconstruction programs. Following the analysis setup presented in the introduction 7.1.1, four classes of input objects to the jet algorithms have been considered: The initial partons of the hard interaction, partons after parton shower (partonic final state, PFS), all stable particles of the hadronic final state (HFS) other than muons or neutrinos and calorimeter towers. The calorimeter towers fulfilling the requirements $E > 0.8\,\text{GeV}$ and $E_\text{T} > 0.5\,\text{GeV}$ were subjected to the same jet algorithms as the generator particles. If necessary a matching of generator and calorimeter jets was performed by looking for the pairs closest to each other in distance $d = \sqrt{(\Delta\Phi)^2 + (\Delta\eta)^2}$.

7.1.5 Jet energy calibration

The jet energy calibration has been performed with a MC calibration method implying calibration factors that are applied on a jet by jet basis to the calorimeter jets depending on pseudo-rapidity η and transverse momentum p_T. The alternative data based technique of gamma-jet calibration where jet transverse energies are measured against recoiling high energetic photons could not yet be employed for this study.

7.1.6 NLO calculation

In order to compare to theoretical predictions of perturbative QCD, calculations of at least next-to-leading order (NLO) precision are required. Here, the program CLOSET++ [184] is employed for the NLO calculation. However, since precise computations in NLO are very time consuming, a more efficient set-up in the form of the fastNLO project [185] is used which allows the fast rederivation of the considered cross section for arbitrary input PDFs and α_S values. This is done by separating the PDF dependency from the hard matrix element calculation by interpolating the PDFs between fixed support points in fractional proton momentum x so that the PDF dependency can be evaluated a posteriori from one complete calculation.

Note that neither PYTHIA nor CLOSET++ contain electroweak corrections which may change high p_T cross sections from $1\,\text{TeV}$ onwards by up to 30% [186]. Insofar this study is consistent, but before comparing to real data this has to be taken into account.

7.1.7 Experimental and theoretical uncertainties

From the experience at the Tevatron [177, 187, 188], it is known that the jet energy scale with an uncertainty of 3% represents by far the dominant source of uncertainty for high p_T jet cross sections. Similarly, PDF uncertainties lead to the dominant uncertainty of the jet cross sections from the theoretical side.

According to CMS studies the jet energy scale in this analysis has been varied by $\pm 3\%$ in order to estimate the impact on the cross section determination. Figure 7.3 presents on the left hand side the corresponding relative experimental uncertainty on the jet cross section for three regions in rapidity. Starting at about 15% at low p_T it rises up to about 50% at high p_T for central rapidity. In the two non-central rapidity regions the uncertainties are of comparable size below about $1\,\text{TeV}$ of transverse momentum, but get considerably larger for higher p_T. In general, a similar behaviour as expected from Tevatron results is observed.

By evaluating the cross section calculation for the error set of the CTEQ6M [12] PDFs the ensuing theoretical uncertainty as shown in figure 7.3 on the right hand side could be derived. It is of the same order of magnitude as the energy scale uncertainty and rises from about 5% for low transverse momenta with a minimum of 3% at $\approx 200\,\text{GeV}$ up to $+65\%$ and -30% at the highest transverse momenta for central rapidity.

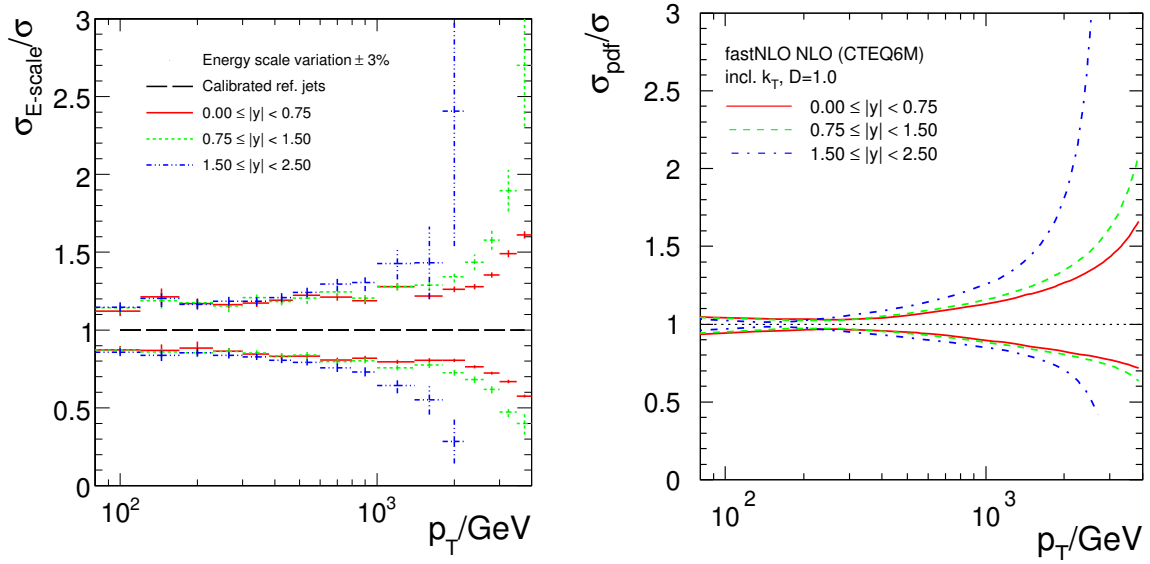

Figure 7.3: Relative systematic uncertainties of the jet cross sections for the k_T algorithm versus p_T due to a change in energy scale of $\pm 3\%$ for three bins in rapidity (left). The error bars represent the statistical uncertainty. On the right hand side, the relative uncertainties due to an evaluation of the error sets of the CTEQ6M [12] PDFs are shown for the same regions in rapidity.

7.1.8 Summary and outlook

The dominant experimental and theoretical uncertainties on the differential inclusive cross sections of jets with high transverse momentum ranging from $80\,\text{GeV}$ up to $4000\,\text{GeV}$ have been investigated. A variation of $\pm 3\%$ in the jet energy scale results in an uncertainty of the derived jet cross sections of 15% at low transverse momenta, increasing up to about 50% at the highest p_T for central rapidity. The theoretical uncertainty due to the parton density functions of the proton has been found to be of the same order of magnitude and rises from about 5% for low transverse momenta with a minimum of 3% at $\approx 200\,\text{GeV}$ up to $+65\%$ and -30% at the highest transverse momenta. For higher rapidities both uncertainties are considerably larger. The results shown have been derived with the k_T jet algorithm, similar values were obtained with the midpoint cone algorithm.

For transverse momenta below about $500\,\text{GeV}$ further sources of uncertainties may give significant contributions to the total uncertainty, e.g. corrections due to pile-up, the underlying event and multiple interactions or hadronisation. Theoretical contributions due to scale variations are of the order of 5% (10% for transverse momenta larger than 3 GeV) for rapidities y below 1.5. Above a rapidity of 1.5 they might be larger especially at the edge of the phase space. In addition, contributions due to α_S and electroweak corrections have to be included before comparing to real data.

In the future, it will be possible to run simultaneous fits of α_S and the parton density func-

tions, especially the gluon density at high x, to the data. To be less sensitive to the jet energy scale other jet related quantities, e.g. jet rates, will be considered. By including other processes into the fit procedure, like W/Z production as a luminosity measure or Drell-Yan reactions to fix the low x gluon density, powerful combined PDF fits to the data of one experiment will become possible.

7.2 Underlying event studies

7.2.1 Definition of the physics process and status of the art

The "Underlying Event" (UE) in a hard scattering process is everything accompanying an event but the hard scattering component of the collision. A CDF analysis [189, 190] showed that the density of particles in the UE of jet events is about a factor of two larger than the density of particles in a typical Minimum Bias (MB) collision. At the LHC the difference might be even larger.

Hard scattering collider events have a distinct topology and one can use the topological structure of the collision to define regions of the η-ϕ space that are sensitive to the UE components of the interaction. By comparing different processes such as high transverse momentum jets, "back-to-back" dijet production, or Drell-Yan, one can partially isolate the various components contributing to the UE.

Multiple parton interaction (MPI) models [191], extending the QCD perturbative picture to the soft regime, turn out to be particularly adequate to describe the physics of the UE. In the framework of these models one can regard the observed differences between the UE in a hard scattering process and a MB collision as the effect of the increased probability of partonic interactions for small impact parameter hadron-hadron collisions: one hard scattering implies a small impact parameter collision which makes it more likely that an additional parton-parton interaction will occur. Also, a hard scattering promotes initial and final state gluon radiation which inevitably contributes to the UE.

Examples of MPI models are implemented in the general purpose simulation programs PYTHIA [68], JIMMY [192], and SHERPA [193]. Other successful descriptions of UE and MB at hadron colliders are achieved by alternative approaches like PHOJET [194], which rely on both perturbative QCD and the Dual Parton Models (DPM). The purely phenomenological description available in HERWIG [195] provides a very useful reference of a model not implementing multiple interactions.

The QCD models considered in this study are different settings, called tunes, of relevant parameters in HERWIG and PYTHIA 6.2. One of the PYTHIA tunes is the ATLAS tune [196] and the other (PY Tunes DW) is a tune by R. Field which is similar to PYTHIA Tune A [197]. All these tunes use the CTEQ5L parton distribution functions. Details of the settings are given in reference [198].

Both Tune A and Tune DW fit the CDF Run 1 and Run 2 UE data [189, 190]. Tune DW also fits the CDF Run 1 Z-boson transverse momentum distribution [199]. Both Tune A and Tune DW use the same multiple parton interaction energy dependence parameter PARP(90) $= 0.25$, while the ATLAS tune uses the default value of 0.16.

The analyses summarised in this section are described in detail in reference [198].

7.2.2 Underlying event observables discussed for charged jet events

Charged jets are constructed from the charged particles using a simple clustering algorithm and then the direction of the leading charged particle jet is used to isolate regions of η-ϕ space that are sensitive to the UE. As illustrated in Figure 7.4, the direction of the leading charged particle jet, chgjet1, is used to define correlations in the azimuthal angle, $\Delta\phi$. The angle $\Delta\phi = \phi - \phi_{\mathrm{chgjet1}}$ is the relative azimuthal angle between a charged particle and the direction of chgjet1. The "transverse" region is almost perpendicular to the plane of the hard 2-to-2 scattering and is therefore very sensitive to the UE. We restrict ourselves to charged particles in the central region $|\eta| < 1$ and consider two p_{T} thresholds, the nominal CMS cut $p_{\mathrm{T}} > 0.9\,\mathrm{GeV/c}$ and a lower threshold with $p_{\mathrm{T}} > 0.5\,\mathrm{GeV/c}$.

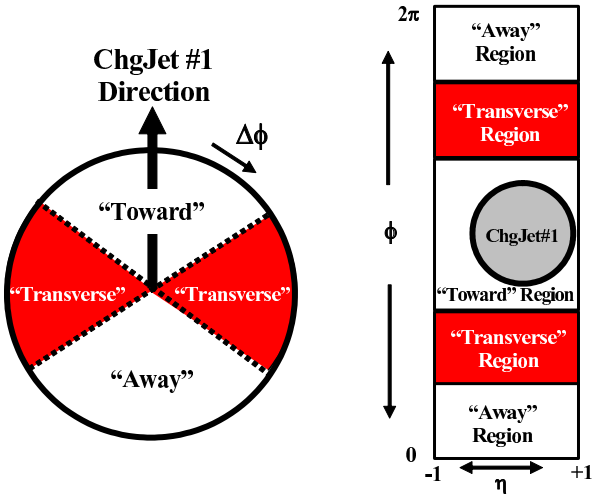

Figure 7.4: Illustration of correlations in azimuthal angle ϕ relative to the direction of the leading charged particle jet ($R = 0.7$) in the event, chgjet1. The angle $\Delta\phi = \phi - \phi_{\mathrm{chgjet1}}$ is the relative azimuthal angle between charged particles and the direction of chgjet1. The "transverse" region is defined by $60^\circ < |\Delta\phi| < 120^\circ$ and $|\eta| < 1$. We examine charged particles in the range $|\eta| < 1$ with $p_{\mathrm{T}} > 0.5\,\mathrm{GeV/c}$ or $p_{\mathrm{T}} > 0.9\,\mathrm{GeV/c}$.

Figure 7.5 shows the QCD Monte Carlo models predictions for the average density of charged particles, $dN_{chg}/d\eta d\phi$, and the average charged PT_{sum} density, $dPT_{sum}/d\eta d\phi$, respectively, in the "transverse" region for $|\eta| < 1$ with $p_{\mathrm{T}} > 0.5\,\mathrm{GeV/c}$ and $p_{\mathrm{T}} > 0.9\,\mathrm{GeV/c}$ versus the transverse momentum of the leading charged particle jet. The charged particle density is constructed by dividing the average number of charged particles per event by the area in η-ϕ space (in this case $4\pi/3$). The charged PT_{sum} density is the average *scalar* p_{T} sum of charged particles per event divided by the area in η-ϕ space.

Due to the multiple parton interactions the PYTHIA tunes rise rapidly and then reach an approximately flat "plateau" region. At very high $P_T(\mathrm{chgjet1})$ they begin to rise again due to initial and final state radiation which increases as the Q^2 scale of the hard scattering increases. HERWIG has considerably fewer particles in the "transverse" region and predicts a steady rise resulting from initial and final state radiation. The ATLAS tune predicts a larger charged particle density than PYTHIA Tune DW for $p_{\mathrm{T}} > 0.5\,\mathrm{GeV/c}$. However, the ATLAS tune and Tune DW have similar charged particle densities for $p_{\mathrm{T}} > 0.9\,\mathrm{GeV/c}$. This is because the ATLAS tune has a "softer" charged particle p_{T} distribution than Tune DW.

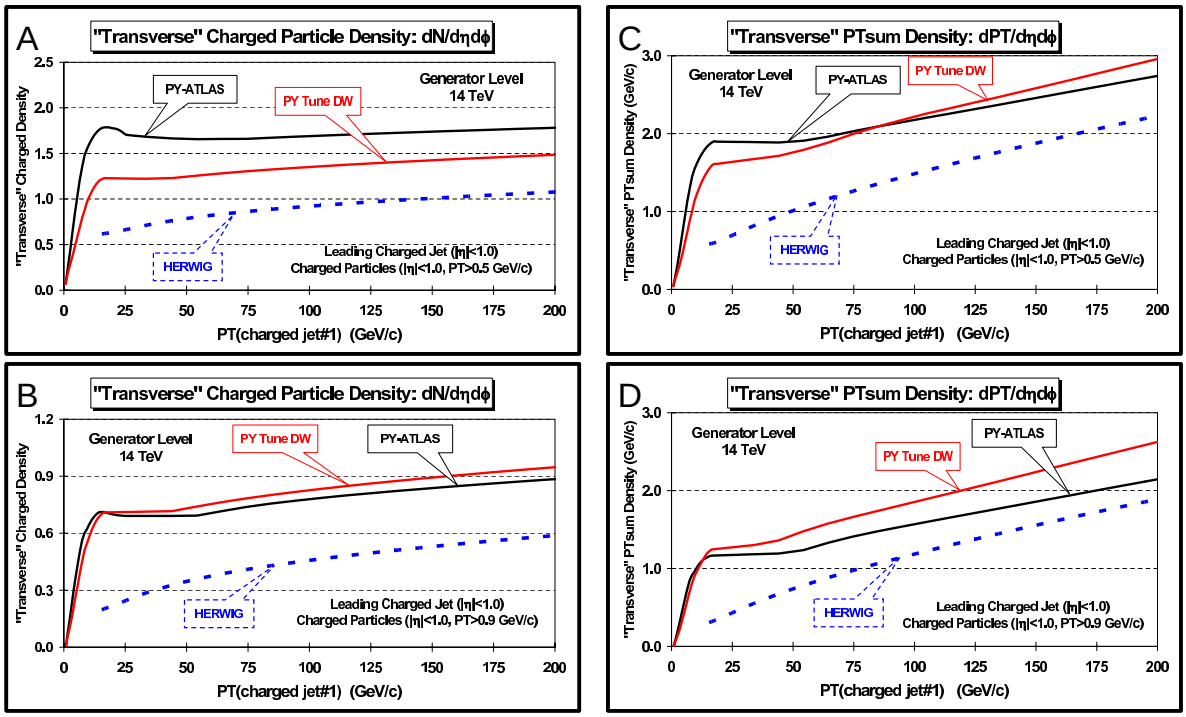

Figure 7.5: QCD Monte Carlo models predictions for charged particle jet production at 14 TeV. *Left*: Average density of charged particles, $dN_{chg}/d\eta d\phi$, with $|\eta| < 1$ in the "transverse" region versus the transverse momentum of the leading charged particle jet for $p_{\mathrm{T}} > 0.5$ GeV/c (*A*) and $p_{\mathrm{T}} > 0.9$ GeV/c (*B*). *Right*: Average charged PT_{sum} density, $dPT_{sum}/d\eta d\phi$, with $|\eta| < 1$ in the "transverse" region versus the transverse momentum of the leading charged particle jet for $p_{\mathrm{T}} > 0.5$ GeV/c (*C*) and $p_{\mathrm{T}} > 0.9$ GeV/c (*D*). The QCD models are HERWIG and two PYTHIA 6.2 tunes described in the text.

7.2.3 Feasibility studies

Here we concentrate on the UE measurement that will be performed in nominal CMS conditions at low luminosity [198]. All the studies presented in this section have been obtained applying the GEANT-4 based simulation and reconstruction chain of the CMS experiment.

Events corresponding to Drell-Yan dimuon pairs and leading QCD processes with superimposed low luminosity pile-up have been generated with PYTHIA 6.2 in different $\hat{p}_{\mathrm{T}}$ regions. The relevant PYTHIA 6.2 parameters adopted by CMS in simulation production are documented in [200]. The triggers used to collect Jet and Drell-Yan samples are described in reference [75].

Charged track reconstruction uses the Combinatorial Track Finder [201]. The default algorithm allows to reconstruct tracks with p_{T} above 0.9 GeV/c. However, the same algorithm can be used in special conditions (with reduced thresholds for the seeds) achieving reasonable performances down to 0.5 GeV/c [198]. For $\eta| < 1$, a reconstruction efficiency better than 90% and a fake rate below 1% are quoted for charged tracks with p_{T} above 0.7 GeV/c.

7.2.3.1 The underlying event as observed in charged jet events

The track-based measurement for the scale of the leading interaction allows to keep an acceptable resolution for jet energies below 20 GeV, where the calorimetric measurement is dominated by large systematic uncertainties.

In principle MB could be studied from any data selection, getting rid of the leading pp interaction and performing the reconstruction of all the primary vertices from all the other piled-up pp interactions. However this methodology turns out to be challenging as the resolution on the position of the pp vertices degrades when lowering the total p_{T} of the associated charged tracks. In this study an MB trigger is defined requiring at least a calorimetric jet of $p_{\mathrm{T}} > 20\,\mathrm{GeV/c}$. In order to combine the measurements performed at different leading charged jet scales, on top of the MB trigger, two additional triggers based on the p_{T} of the leading high level trigger jet are adopted: $p_{\mathrm{T}} > 60\,\mathrm{GeV/c}$ and $p_{\mathrm{T}} > 120\,\mathrm{GeV/c}$, which will be referred to as JET60 and JET120. Jets are reconstructed with an iterative cone algorithm of radius 0.5 in the pseudorapidity-azimuth space.

Tracks arising from the piled-up interactions are suppressed requiring the extrapolated coordinate along the beam axis to be inside 1 mm with respect to the primary vertex associated to the leading charged jet. The selection of the pp interaction with the highest p_T charged jet tends to create a small bias on the MB sample, reducing the statistics available at very low $P_T(\mathrm{chgjet1})$.

The definition of the main UE observables have been introduced in section 7.2.2. The density of charged particles, $dN_{chg}/d\eta d\phi$, and the charged PT_{sum} density, $dPT_{sum}/d\eta d\phi$, with $p_{\mathrm{T}} > 0.9\,\mathrm{GeV/c}$ and $|\eta| < 1$ in the "transverse" region are reported in Figure 7.6. Bins of $2\,\mathrm{GeV/c}$ are used up to $P_T(\mathrm{chgjet1}) = 20\,\mathrm{GeV/c}$ and bins of $10\,\mathrm{GeV/c}$ above.

The shapes of uncorrected reconstruction level distributions basically agree with the corresponding generator level ones. The difference in absolute scale (about -20% for both $dN_{chg}/d\eta d\phi$ and $dPT_{sum}/d\eta d\phi$) turns out to be compatible with charged track inefficiencies and fake rates. Further details on these systematic effects, including the calibration and resolution of the leading charged jet have been studied in [198].

Figure 7.6 shows also the ratio between the observables for $p_{\mathrm{T}} > 0.9\,\mathrm{GeV/c}$ and $p_{\mathrm{T}} > 0.5\,\mathrm{GeV/c}$ in the "transverse" region. These ratios, which are sensitive to the differences between the models and/or to the choice of the tuning for a given model, are also nicely free from the systematic effects enumerated above, and basically do not need to be corrected when comparing to the corresponding generator level observables.

7.2.3.2 The underlying event as observed in Drell-Yan muon-pair production

Drell-Yan muon pair production provides an excellent way to study the UE. Here one studies the outgoing charged particles (excluding the $\mu^+\mu^-$ pair) as a function of the muon-pair invariant mass. After removing the muon-pair everything else is the UE. As for the charged jet production, we restrict ourselves to charged particles in the central region $|\eta| < 1$ and consider the two p_{T} thresholds $p_{\mathrm{T}} > 0.5\,\mathrm{GeV/c}$ and $p_{\mathrm{T}} > 0.9\,\mathrm{GeV/c}$.

Single muon and muon-pair CMS triggers ensure very high efficiencies for the studied process. The relative mass shift and the corresponding resolution of the reconstructed muon-pair are studied in detail in reference [198]. Tracks arising from the piled-up interactions are suppressed requiring the extrapolated coordinate along the beam axis to be inside 1 mm with respect to the primary vertex associated to the leading muons.

In our study, we require "isolated muons", not to have charged tracks with $p_{\mathrm{T}} > 0.9\,\mathrm{GeV/c}$ in a cone of radius $\mathrm{R} = \sqrt{(\Delta\phi)^2 + (\Delta\eta)^2} = 0.3$ in the azimuth-pseudorapidity space centred along the direction of the muon. Selecting isolated muons turns out to be essential to reduce the QCD background to negligible levels for $p_{\mathrm{T}} > 15\,\mathrm{GeV/c}$, while keeping an efficiency of

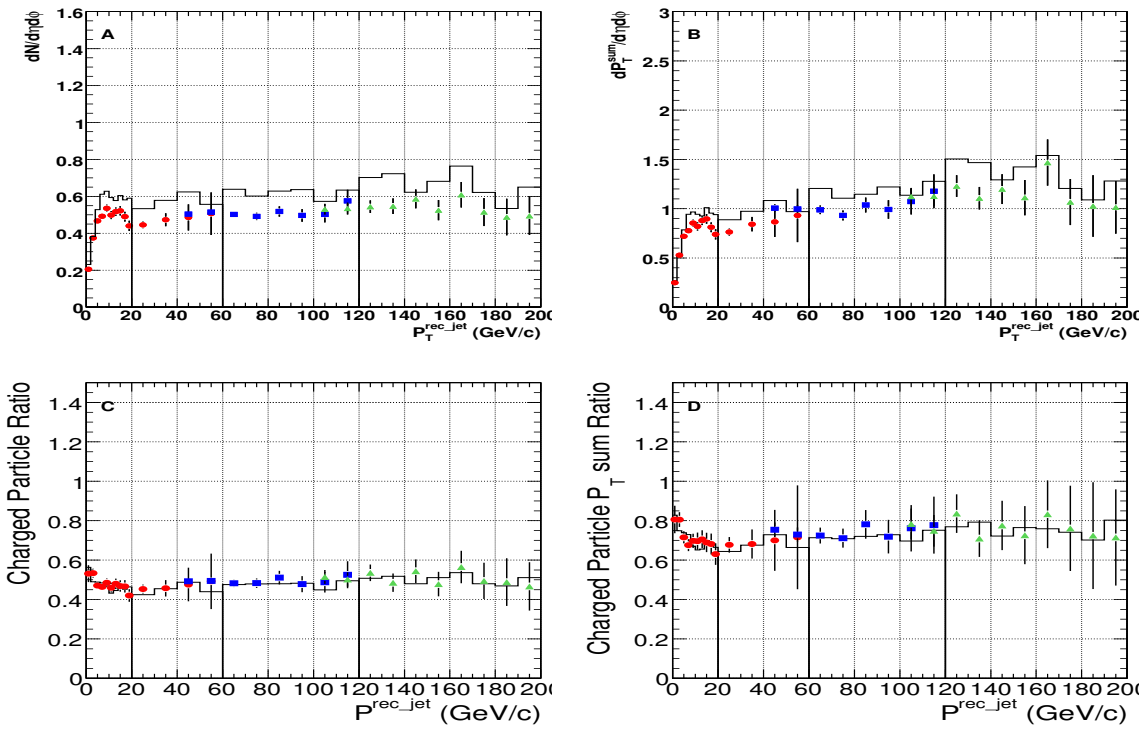

Figure 7.6: Charged jet production at 14 TeV. Charged tracks with $|\eta| < 1$ in the "transverse" region. Density of charged particles, $dN_{chg}/d\eta d\phi$ (*A*) and PT_{sum} density, $dPT_{sum}/d\eta d\phi$ (*B*), with $p_{\mathrm{T}} > 0.9\,\mathrm{GeV/c}$ versus the transverse momentum of the leading charged particle jet. Ratio between density of charged particles with $p_{\mathrm{T}} > 0.9\,\mathrm{GeV/c}$ and $p_{\mathrm{T}} > 0.5\,\mathrm{GeV/c}$ (*C*) and ratio between PT_{sum} density with $p_{\mathrm{T}} > 0.9\,\mathrm{GeV/c}$ and $p_{\mathrm{T}} > 0.5\,\mathrm{GeV/c}$ (*D*) versus the transverse momentum of the leading charged particle jet. Data from different triggers are superimposed: (*circles*) = Minimum Bias; (*squares*) = JET60; (*triangles*) = JET120. The lines show the generator level distributions; the points with error bars correspond to the raw (uncorrected) reconstruction level distributions.

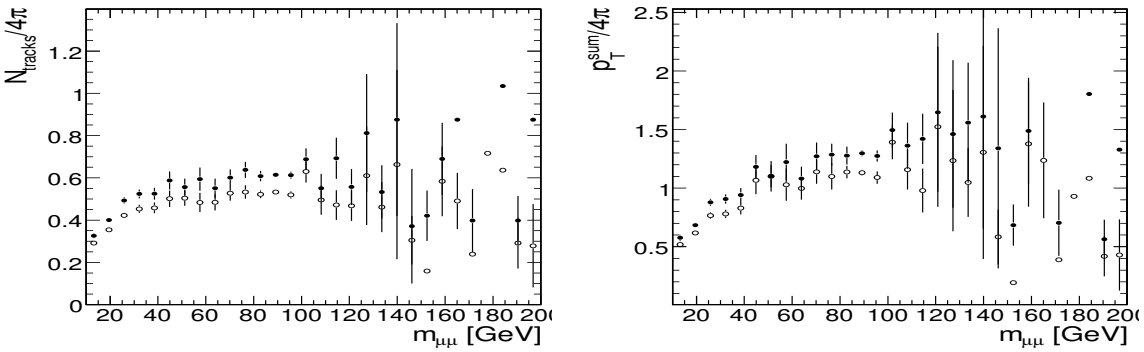

Figure 7.7: Muon-pair production at 14 TeV with two isolated muons. Density of charged particles, $dN_{chg}/d\eta d\phi$ (*left*), PT_{sum} density, $dPT_{sum}/d\eta d\phi$ (*right*), with $p_{\mathrm{T}} > 0.9\,\mathrm{GeV/c}$ and $|\eta| < 1$ versus the muon-pair invariant mass. (*full circles*) correspond to the generator level distributions; (*empty circles*) correspond to the raw (uncorrected) reconstruction level distributions.

76.9% for Drell-Yan muon-pairs in the same p_{T} region.

The charge particle density, $dN_{chg}/d\eta d\phi$, and the charged PT_{sum} density, $dPT_{sum}/d\eta d\phi$ with $p_{\mathrm{T}} > 0.9\,\mathrm{GeV/c}$ and $|\eta| < 1$ in muon-pair production with isolated muons versus the muon-pair invariant mass are shown in Figure 7.7. Correlations between isolation and UE activity have been studied in references [63, 198].

7.2.4 Conclusions

Predictions on the amount of activity in UE at the LHC based on extrapolations from the lower energy data differ greatly. In this study we have demonstrated the feasibility of reference UE measurements at CMS under nominal conditions, assessing our capability to distinguish between the predictions of different models. The UE is studied by examining charged particles in the "transverse" region in charged particle jet production and in the central region of Drell-Yan muon-pair production (after removing the muon-pair).

7.3 Physics of b-quarks and hadrons

7.3.1 Inclusive b-quark production

7.3.1.1 Introduction

At the LHC new opportunities to improve our understanding of the physics of b quarks will become available because of the high statistics data samples and the high centre-of-mass energy. A study [202] has been performed to investigate methods in CMS of identifying b jets (b "tagging") in an inclusive sample of events containing jets and at least one muon. Here we present the capability to measure the inclusive b quark production cross section as a function of the B-hadron transverse momentum and pseudorapidity. An important result of our study is an estimate for the B-hadron p_{T} range reachable at LHC.

Inclusive b-quark production has been studied at other proton and electron colliders. The observed shapes of distributions and correlations are reasonably well explained by perturbative QCD. However, the observed cross-sections at the Tevatron (Run I) are larger than QCD predictions [203–210] which is confirmed by Run II data. Similar effects are observed in $\gamma\mathrm{p}$ collisions at HERA [211–217] and in $\gamma\gamma$ interactions at LEP [218, 219].

The agreement between experiment and theory has improved due to more precise parton density functions and proper estimates of fragmentation effects [220–225]. But the agreement is not complete and the improvement of the phenomenological description is required using also experimental input.

7.3.1.2 Analysis

This study of the CMS capability to measure the inclusive b production is based on full detector simulation. The generated events are passed through the GEANT4 simulation of CMS. Pile-up corresponding to low-luminosity LHC running conditions ($\mathcal{L} = 2 \times 10^{33}\,\mathrm{cm^{-2}\,s^{-1}}$) is also generated.

7.3.1.2.1 Event selection About 4 million signal and background events were processed, mainly with high transverse momentum of the partons ($p_{\mathrm{T}} > 50\,\mathrm{GeV/c}$). Samples of QCD jets were used. Jets in those samples cover the full geometrical acceptance in pseudorapidity of the tracking detector, $|\eta| < 2.4$. The measurement of the differential cross sections is studied for B-hadrons of $p_{\mathrm{T}} > 50\,\mathrm{GeV/c}$ and within the fiducial volume of $|\eta| < 2.4$. First,

the events are required to pass the Level-1 (L1) trigger selection for the single muon trigger stream which accepts events with muons having $p_{\mathrm{T}} > 14\,\mathrm{GeV/c}$. The most energetic B-hadron inside the phase space defined above is selected. The trigger efficiency is flat as a function of the B-hadron pseudorapidity within the Level-1 trigger acceptance of $|\eta| < 2.1$. It increases with transverse momentum of the B-particle. The average Level-1 trigger efficiency corresponds to the expected value of the branching fractions for the semi-leptonic b quark and c quark decays, about 19% [54]. At Level-1, the single muon trigger is used. At the High Level Trigger (HLT) we require the "muon + b-jet" trigger, fired by non-isolated muons with $p_{\mathrm{T}} > 19\,\mathrm{GeV/c}$ and by jets with $E_{\mathrm{T}} > 50\,\mathrm{GeV/c}, |\eta| < 2.4$ and compatible with b tagging.

The event selection requires a b-tagged jet in the fiducial volume to be present in the event. B tagging is based on inclusive secondary vertex reconstruction in jets [156]. The tagging algorithms combine several topological and kinematic secondary vertex related variables into a single tagging variable to discriminate between jets originating from b quarks and those from light quarks and gluons.

To measure differential cross sections for inclusive B-particle production as a function of its transverse momentum p_{T} and pseudorapidity η, $d\sigma/dp_{\mathrm{T}}$ and $d\sigma/d|\eta|$, we select as the reconstructed B-particle candidate the most energetic b tagged jet. Good correspondence between the generated B-particle and the reconstructed b-tagged jet is observed. The corresponding p_{T} and pseudorapidity relative resolutions are shown in Figure 7.8 for B-particles with $p_{\mathrm{T}} > 170\,\mathrm{GeV/c}$. The resolutions are 13% and 6% for p_{T} and pseudorapidity, respectively.

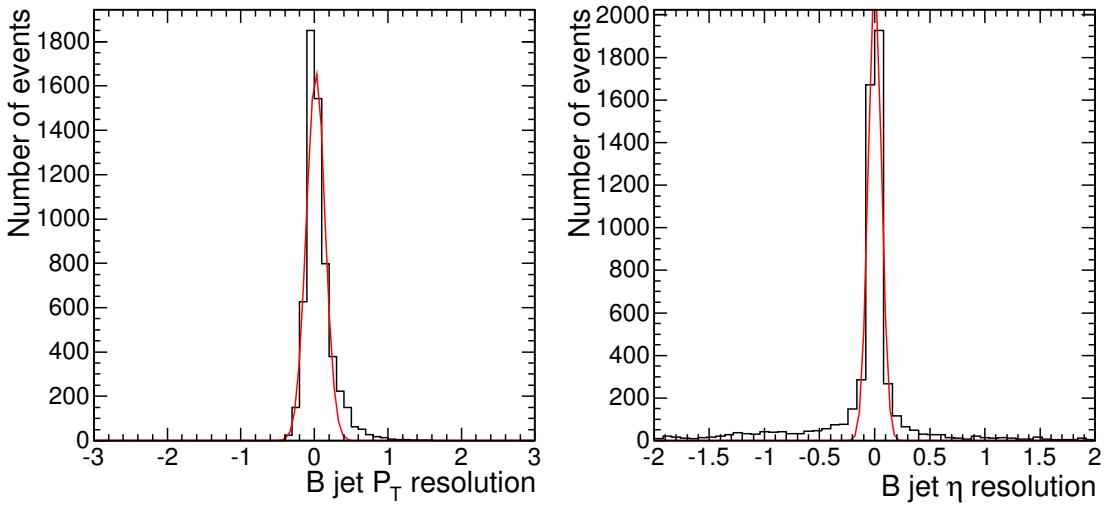

Figure 7.8: Relative resolution, (Reconstructed − True) / True, for p_{T} and pseudorapidity of b tagged jets in CMS.

The efficiency of the b tagging by secondary vertices in jets is shown in Figure 7.9 as function of the B-particle transverse momentum and pseudorapidity. The b tagging efficiency is defined with respect to events passing the Level-1 trigger and with a single muon of $p_{\mathrm{T}} > 19\,\mathrm{GeV/c}$ selected. The efficiency decreases with increasing transverse momentum, while being rather flat as function of pseudorapidity. The slow degradation for larger transverse momenta is caused by the worsening of the tracking resolution with increasing p_{T}, an increased track multiplicity from fragmentation and more difficult pattern recognition in

dense jets. The average b tagging efficiency is 65% in the barrel region, while the efficiency is about 10 % less for the endcap region. The muon plus b-jet cross-channel trigger has a 4.3 Hz rate for the signal and a 6.1 Hz total event rate [202]. This trigger rate corresponds to a low-luminosity LHC run at $\mathcal{L} = 2 \times 10^{33}\,\mathrm{cm}^{-2}\,\mathrm{s}^{-1}$.

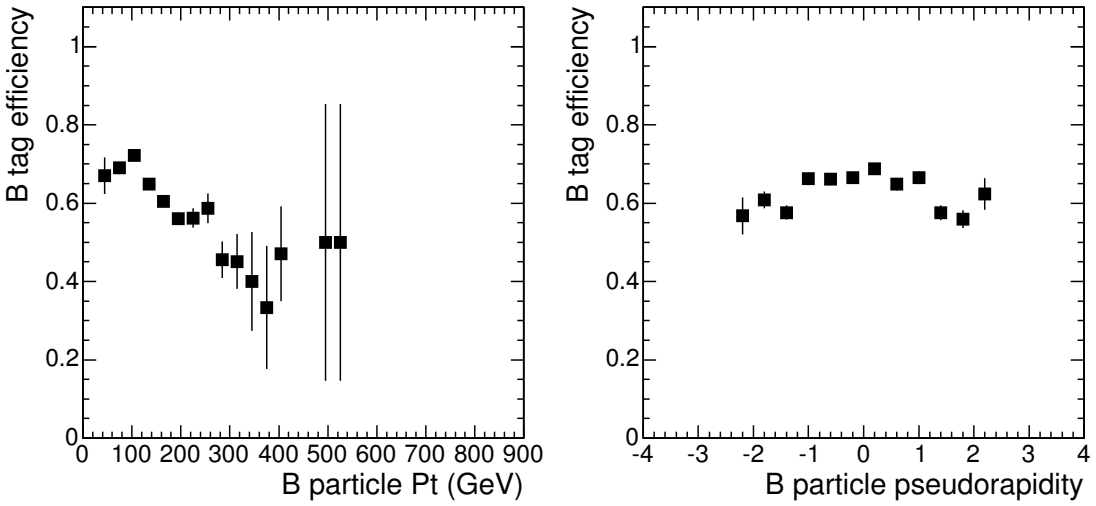

Figure 7.9: The b tagging efficiency versus p_{T} and pseudorapidity of the generated B-particle.

To measure the cross section one needs to know the number of selected events, the integrated luminosity, the event sample purity (signal fraction) and the signal efficiency. The signal fraction can be determined from the simulated prediction of the background contribution to the selected event sample. In order to rely less on the absolute prediction for the background one can extract the signal fraction using the prediction of the signal and background shapes for some sensitive variables. A fit to the data distribution using the simulated shapes for the signal and background is performed. To do so we apply a lepton tag by selecting inclusive muons.

7.3.1.2.2 Muon tag Muons are reconstructed in the muon chambers, matched to the inner tracker information and refitted using both subdetectors information. This provides the most precise muon track measurement. Each reconstructed muon is associated to the most energetic b tagged jet. The muon must be closer to this b tagged jet than to any other jet in the event. Otherwise the event is discarded.

In most cases the tagged muon is inside the b jet. The average efficiency of associating the muon with the b tagged jet is 75 %.

7.3.1.2.3 Results We calculate the transverse momentum of the muon with respect to the b-jet axis which effectively discriminates between b events and background. The slopes of the p_{T} spectra are very different and this is exploited in the fit of the selected events to determine the fractions of the muon sources in the sample.

Figure 7.10 shows an example of the fit of the distribution of the muon p_{T} with respect to the closest jet, using the expected shapes for the muons from b events, charm events and light quark events. The normalisation of the three contributions are free parameters in the

fit. The events in this plot are from a sample of QCD events generated with the PYTHIA "p_{T}-hat" parameter in the range $230 < \hat{p_{\mathrm{T}}} < 300\,\mathrm{GeV/c}$. In the fit the shapes of the distributions were fixed using an independent QCD sample generated with $170 < \hat{p_{\mathrm{T}}} < 230\,\mathrm{GeV/c}$. The fit results as well as the Monte Carlo input are quoted in Table 7.1. The event fractions are well reproduced within statistical errors. In the actual experiment the shapes will be verified using data at different selection stages. Also the background shape will be derived from the data itself by applying an anti-tag selection (b-suppressed event sample).

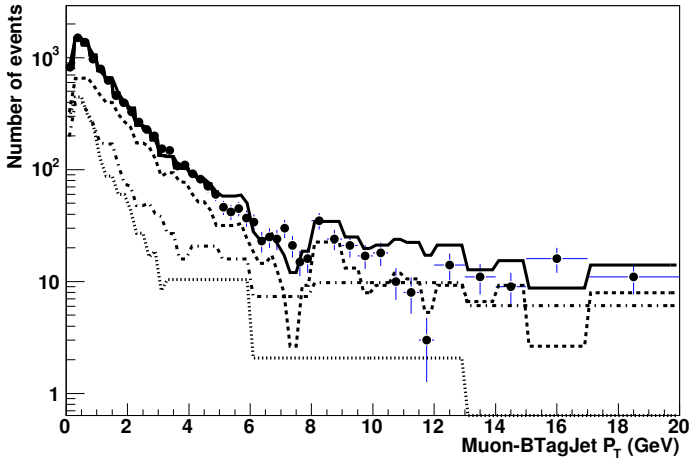

Figure 7.10: Fit of the muon p_{T} spectrum with respect to the closest b tagged jet. The sample of generated QCD events with "p_{T}-hat" parameter in the range $230 < \hat{p_{\mathrm{T}}} < 300\,\mathrm{GeV/c}$ is tested. The contributions of tagged muons from b events (dashed curve), c events (dot-dashed curve) and light quark events (dotted curve) as defined by the fit are shown. The solid curve is the sum of the three contributions.

Table 7.1: Results of the fit to the distribution of the transverse momentum of the muon with respect to the nearest b tagged jet. The number of beauty, charm and light quark events in the Monte Carlo input are compared to the fit result.

	MC input, $230 < \hat{p_{\mathrm{T}}} < 300\,\mathrm{GeV/c}$	Fit result
$N_{\mathrm{b\bar{b}}}$	5250	5222 ± 501
$N_{\mathrm{c\bar{c}}}$	2388	2050 ± 728
N_{uds}	1740	1778 ± 341

In Table 7.2 the b purity, $c\bar{c}$ and light quark event fractions for the different QCD samples are shown. The b purity decreases from about 70 % down to 55 % from low p_{T} events to the high transverse momentum events. The expected number of $b\bar{b}$ events after event selection is quoted for $10\,\mathrm{fb}^{-1}$ of integrated luminosity. For the phase space of $p_{\mathrm{T}} > 50\,\mathrm{GeV/c}$ and $|\eta| < 2.4$ the event selection will allow for a b event statistics of about 16 million events. We conclude that for B-hadrons a p_{T} range up to 1.5 TeV/c will be accessible with the CMS detector at the LHC.

The background contribution from $t\bar{t}$ events has been estimated from a sample of one million simulated events including all decay modes. The total number of $t\bar{t}$ events passing the selection amounts to 104 thousand events for $10\,\mathrm{fb}^{-1}$ of integrated luminosity, corresponding

Table 7.2: B purity and expected number of events after final event selection. The expected number of $b\bar{b}$ events is quoted for $10\,\mathrm{fb}^{-1}$ of integrated luminosity.

$\hat{p_{\mathrm{T}}}$, GeV/c	$\mathrm{N}^{\mathrm{QCD}}_{\mathrm{generated}}$	$b\bar{b}$ purity, %	$c\bar{c}$ fraction, %	uds fraction, %	$\mathrm{N}^{\mathrm{b\bar{b}}}_{\mathrm{expected}}$
$50-80$	198993	66	32	2	1.4 M
$80-120$	294986	66	32	2	6.1 M
$120-170$	291982	72	26	2	5.1 M
$170-230$	355978	71	26	3	2.4 M
$230-300$	389978	73	24	3	0.9 M
$300-380$	283983	70	25	5	0.3 M
$380-470$	191989	68	27	5	88 k
$470-600$	190987	64	29	7	34 k
$600-800$	94996	60	31	9	10 k
$800-1000$	89999	60	30	10	2.0 k
$1000-1400$	89998	55	31	14	0.5 k

on average to a less than 1 % background contribution. The $t\bar{t}$ background becomes more pronounced for the high p_{T} part of the inclusive B spectrum. In the region $p_{\mathrm{T}} > 500\,\mathrm{GeV/c}$ it amounts to 2.4 %.

The total event selection efficiency is about 5 %. By correcting for the semi-leptonic branching ratio of b quarks and c quarks it amounts to about 25 % on average. It turns out that the total efficiency is almost independent of transverse momentum and angle of the B-particle. Therefore the measurement of the differential cross section is less affected by systematic uncertainties due to bin-by-bin efficiency corrections.

7.3.1.2.4 Systematics Uncertainties Several potential sources for systematic uncertainties are considered and their impact on the observed cross section is detailed in Table 7.3. The largest uncertainty arises from the 3 % error on the jet energy scale (see appendix B)

Table 7.3: Sources of systematic uncertainty in % on the inclusive b production cross section measurement. The total systematic uncertainty is calculated by adding all contributions in quadrature.

Source	uncertainty, %
jet energy scale	12
event selection	6
B tagging	5
luminosity	5
trigger	3
muon Br	2.6
misalignment	2
muon efficiency	1
$t\bar{t}$ background	0.7
fragmentation	9
total	18

which leads to a cross section error of 12 % at $E_{\mathrm{T}} > 50\,\mathrm{GeV/c}$. Other important uncertainties arise from the event-selection procedure and the Monte Carlo modelling of the detector

response, including the lepton identification and the detector resolution on the energy and angular variables which identify the fiducial volume. The effect of these systematic uncertainties is estimated by varying the corresponding cuts and repeating the fits for the newly selected event samples. It results in an uncertainty of 6 %. The expected b-tag systematics for $10\,\text{fb}^{-1}$ integrated luminosity is 5 % [7]. The luminosity uncertainty is also 5 % [7].

The trigger efficiency will be determined from the data themselves. We estimate its uncertainty from Monte Carlo studies to be 3.0 %. The experimental uncertainties on the semileptonic branching ratio of b quarks [54] is also propagated to the measurement. The impact of the detector misalignment on the CMS b tagging performance has been investigated in [156]. The effect has been found to be small (2 %). The muon detection efficiency can be determined with better than 1 % precision [7]. The $t\bar{t}$ background subtraction uncertainty is conservatively taken as absolute value of the expected $t\bar{t}$ contribution to the considered phase space.

A large contribution is expected from the fragmentation modelling. We estimate the magnitude of the effect from the DØ b-jet production measurement at Tevatron [210]. This uncertainty propagates to the cross section as a 9 % effect independent of jet E_{T}.

The estimated statistical, systematic and total uncertainty as function of the b tagged jet transverse momentum with respect to the beam line is shown in Figure 7.11.

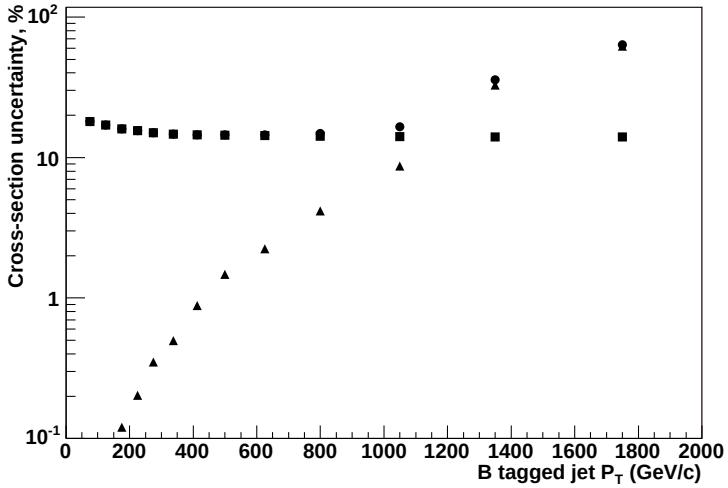

Figure 7.11: The statistical uncertainty for the cross section measurement (triangles), systematic (squares) uncertainty and total (dots) uncertainty as function of the b tagged jet transverse momentum with respect to the beam line. Total uncertainty comprises the statistical and systematic uncertainties added in quadrature.

7.3.1.3 Conclusion

The event selection for inclusive b production measurement at CMS will allow to study b production mechanisms on an event sample of 16 million b events for $10\,\text{fb}^{-1}$ of integrated luminosity. The b purity of the selected events varies as function of the transverse momentum in a range from 70 % to 55 %. Our estimate shows that with the CMS detector we can reach $1.5\,\text{TeV/c}$ as the highest measured transverse momentum of B hadrons.

7.3.2 Study of B_c hadrons

7.3.2.1 Introduction

The B_c meson is the ground state of the $\bar{b}c$ system, which is doubly heavy flavoured. This unique character provides a window for studying heavy-quark dynamics that is very different from the one of quarkonium. The experimental study of B_c will help us to understand heavy quark dynamics and to test the spin symmetry derived in non-relativistic quantum chromodynamics (NRQCD) [226–235]. B_c mesons have been observed at the Fermilab Tevatron collider by the CDF collaboration through the decay channel $B_c \rightarrow J/\psi\ \ell\nu$ [236]. The mass and lifetime are measured to be [237] M(B_c) = $6.40 \pm 0.39(stat) \pm 0.13(sys)$ GeV/c^2 and $\tau(B_c) = 0.46^{+0.18}_{-0.16} \pm 0.03(sys)$ ps, in agreement with the non-relativistic potential model [238–240] and other approaches [241–243].

Because of the higher colliding energy, the production cross section at the LHC is about a factor of 16 [230] larger than at the Tevatron. As also the LHC luminosity will be higher, CMS has the potential to collect much more B_c mesons than the Tevatron experiments do. We propose to study the B_c meson through $B_c \rightarrow J/\psi\pi$, $J/\psi \rightarrow \mu^+\mu^-$. The goal is to measure the mass and lifetime, and to compare the results with theoretical predictions which do have large uncertainties at the moment. More details on the analysis can be found in reference [244].

7.3.2.2 Monte Carlo data samples

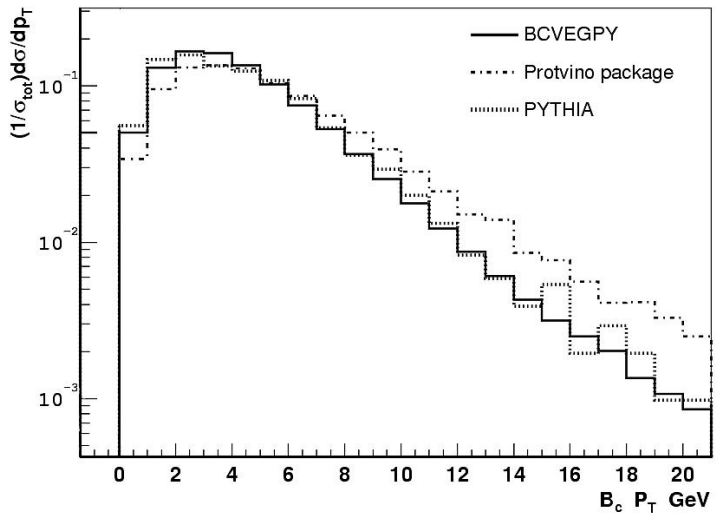

Figure 7.12: Comparison of p_{T} distributions of B_c mesons for the generator BICEPS, Gouz and PYTHIA.

A large amount of Monte Carlo data were produced to study the feasibility for CMS to measure the B_c mass and lifetime with the first fb^{-1}. There are two dedicated B_c generators, one is called BICEPS, developed at ITP, Beijing, by Chang *et al.* [230, 235], and the other is developed at IHEP, Protvino, by Berezhnoy *et al.* [238, 239]. Both packages are based on perturbative QCD, and have been integrated into the SIMUB package [129]. PYTHIA [245] can also generate B_c events, but it takes much more CPU time than the dedicated ones. For comparison, the p_{T} distribution of B_c mesons, generated by PYTHIA, BICEPS and the Protvino package (named Gouz in the plot), are shown in Figure 7.12. One can see that the Protvino

package produces higher p_{T}, while PYTHIA agrees with BICEPS. In order to save CPU time, BICEPS is used to generate B_{c} events. During generation, only events were retained which contain within $|\eta| < 2$ a B_{c} with $p_{\mathrm{T}} > 10\,\mathrm{GeV/c}$, together with a muon of $p_{\mathrm{T}} > 4\,\mathrm{GeV/c}$ within $|\eta| < 2.2$. After the kinematic cuts, the cross section multiplied by the branching ratio is 1.78 pb. 52,000 B_{c} events were produced, corresponding to 29.2 fb^{-1} of integrated luminosity.

Important background sources are J/ψ mesons from decays of other B hadrons and prompt J/ψ mesons. Because of their large cross sections also QCD jets, in particular $b\bar{b} \to \mu^+\mu^- X$, $c\bar{c} \to \mu^+\mu^- X$, as well as $W + \mathrm{jets}$ and $Z + \mathrm{jets}$ have to be considered.

B hadrons that decay into J/ψ were generated with PYTHIA6.228 with kinematic cuts similar to B_{c} production, and prompt J/ψevents were generated by PYTHIA6.324, where the colour-octet contribution is included.

The full CMS detector simulation and reconstruction was applied to the generated samples. The fast simulation package FAMOS was also used to produce the B_{c} events, B hadrons, prompt J/ψ and $c\bar{c} \to \mu^+\mu^- X$ (Table 7.4).

Table 7.4: The cross section multiplied by the branching ratio after kinematic cuts and the number of events produced for B hadrons and prompt J/ψ and $c\bar{c} \to \mu^+\mu^- X$.

channel	σ·Br.(pb)	Nevents
B^0	70.3	740,000
B^+	70.7	740,000
B_s	14.8	190,000
Λ_b	19.4	200,000
prompt J/ψ	240.3	500,000
$c\bar{c} \to \mu^+\mu^-$X	1690	210,000

Samples corresponding to $10\,\mathrm{fb}^{-1}$ of B hadrons, $2\,\mathrm{fb}^{-1}$ of prompt J/ψ and $0.12\,\mathrm{fb}^{-1}$ of $c\bar{c} \to \mu^+\mu^-$X events were produced for the analysis. Additional background samples of about 950,000 QCD, 880,000 $W + \mathrm{jets}$, 710,000 $Z + \mathrm{jets}$ and 100,000 $b\bar{b} \to \mu^+\mu^- X$ events were used.

7.3.2.3 Selection

Signal events should have a b-jet, a c-jet and a B_{c} meson which decays into a J/ψ and a pion, with the subsequent $J/\psi \to \mu^+\mu^-$ decay. The selection starts from 2 muon tracks. The p_{T} of both muons should be larger than 4 GeV/c and the absolute value of η less than 2.2. The two muons should have different charge and share the same vertex. To form a J/ψ candidate the invariant mass of the muons should be in a window between 3.0 and 3.2 $\mathrm{GeV/c^2}$. An additional track must be found at the same vertex of the J/ψ which is inconsistent with a muon or an electron. The p_{T} of it should be larger than 2 GeV/c and the absolute value of η less than 2.4.

The decay length L_{xy}, the proper decay length L_{xy}^{PDL} and the error of the decay length σ_{xy} are calculated from the J/ψ vertex and the primary vertex in the xy-plane. The resolution of the proper decay length is 25 μm. It is found that the resolution is almost independent of the proper decay length. In order to suppress the prompt backgrounds, the second vertex has to be displaced from the primary one. We require $L_{xy}/\sigma_{xy} > 2.5$ and $L_{xy}^{PDL} > 60\,\mu$m. In addition, the condition $\cos\theta_{sp} > 0.8$ is applied where θ_{sp} is the opening angle between the second vertex (pointing from the primary vertex) and the reconstructed B_{c} momentum.

Finally, the reconstructed B_c candidate must be in a mass window between 6.25 and 6.55 GeV/c^2.

The number of B_c and background events for $1\,\text{fb}^{-1}$ after the selection are listed in Table 7.5. The total number of background events was estimated to be 2.6 ± 0.4, mainly from B hadron decays into J/ψ. So far tagging of the b jet is not used in the analysis.

Table 7.5: Estimated number of signal and background events for $1\,\text{fb}^{-1}$.

B_c	B^+	B_s	B_0	prompt J/ψ	Λ_b	$c\bar{c}$	$b\bar{b}$	QCD
120 ± 11	0.7 ± 0.2	0.1	0.9 ± 0.3	0.1	0.1	0.01	0.01	0.7 ± 0.1

Because of the high cross section the number of produced QCD Monte Carlo events is not sufficient to directly determine the QCD background which is therefore estimated in three steps [244]. At first the efficiency to select two muons is obtained directly from the QCD sample, then the efficiency to reconstruct two muons into a J/ψ candidate is calculated from the $c\bar{c} \to \mu^+\mu^- X$ sample, and finally the efficiency for the J/ψ candidate to fake a B_c meson is obtained from the prompt J/ψ sample. The probability of a QCD event to pass the selection cuts is then approximated as the product of the above three efficiencies. In this way, the total number of QCD background for 1 fb^{-1} is estimated to be 0.7 events.

This study which is aimed at the first fb^{-1} collected with the CMS detector assumes that in this initial phase the dimuon trigger threshold can be set at values such that the applied cut of $p_T > 4$ GeV/c on both muons does not introduce a significant inefficiency at trigger level. In case the available trigger bandwidth will prohibit this, more sophisticated High Level Trigger algorithms like a J/ψ mass window could be invoked to restore the trigger efficiency. A detailed study is underway.

7.3.2.4 Mass and lifetime fitting

A kinematic fit was applied to the selected events imposing a J/ψ mass constraint and forcing the two muon tracks as well as the pion track to share the same vertex. After the kinematic fit the invariant mass of the J/ψ – pion system is shown in Figure 7.13. A Gaussian fit provides a mean value of 6406 MeV/c^2, close to the input of 6400 MeV/c^2, and a mass resolution of 22 MeV/c^2. The number of signal events in the plot for $1\,\text{fb}^{-1}$ is 120. Backgrounds from B hadrons and prompt J/ψ are included in the plot, while other backgrounds are neglected here.

A binned likelihood fit was done on the proper decay length distribution of the selected B_c events with the likelihood defined as $L = \prod P(n_i, \mu_i)$. $P(n_i, \mu_i)$ denotes the Poisson distribution with n_i events observed and μ_i events predicted in the i-th bin:

$$\mu = N \cdot \epsilon(x) \cdot \exp(-x/c\tau) \otimes G(x, \sigma)$$

Here x represents the proper decay length, N and $c\tau$ are the parameters to be fitted and $G(x, \sigma)$ is a Gaussian smearing function with σ fixed to $25\,\mu$m which is the resolution of the proper decay length. The efficiency $\epsilon(x)$ is obtained from the large B_c sample.

The result of the fit is $c\tau = 148.8 \pm 13.1\,\mu$m which is consistent with the used input value of $150\,\mu$m. The distribution of the proper decay length together with the fit result is shown in Figure 7.13.

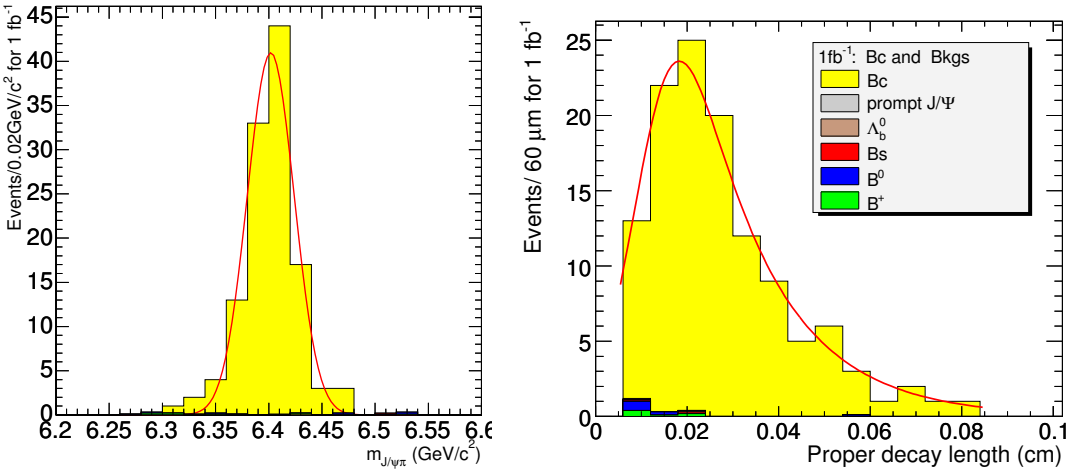

Figure 7.13: Left: The invariant mass of the J/ψ and pion candidate for the selected B_c. Right: The B_c proper decay length distribution. Both plots correspond to 1 fb^{-1}.

7.3.2.5 Systematic uncertainty

The influence of imperfect detector alignment which is of particular importance at the beginning of the CMS experiment on the track and vertex reconstruction has been studied in [98, 139]. It will affect the study of B_c in three ways: the momentum scale of muons and pions, the mass resolution and finally the vertex precision. Taking the scale uncertainty to be $\Delta(1/p_T) = 0.0005/$ GeV/c, the resulting uncertainties on the B_c mass is 11 MeV/c^2 and $0.2\,\mu$m on $c\tau$.

The effect of the muon momentum resolution was estimated following [98] and muon p_T-values of $10, 100$ and 1000 GeV/c were studied for different η. The Δp_T to be smeared for a muon track from B_c was extrapolated from its p_T and η according to [98]. The resulting B_c mass uncertainty is 10 MeV/c^2, and $0.8\,\mu$m on $c\tau$. The error from the vertex uncertainty was determined according to [139] causing an uncertainty on $c\tau$ of $2.4\,\mu$m.

The uncertainty on the efficiency as function of the proper decay length origins from the limited Monte Carlo statistics. By subtracting $\sqrt{N}$ events from the sample ($N = 3600$ events), new efficiencies were calculated and the fit was repeated. The observed difference of $0.1\,\mu$m on $c\tau$ is taken as systematic uncertainty.

The theoretical uncertainty was estimated from Figure 7.12 which shows the p_T distributions from different generator packages. The B_c events, generated by BICEPS, were reweighted to agree with the Gouz distribution and the analysis was repeated. The difference on $c\tau$ was found to be $1.5\,\mu$m which is taken as the error from this source.

To check the sensitivity on the cuts, the muon and pion p_T cuts were changed by one standard deviation of their resolution, about 1.5% depending on η. Other cuts like on $\cos\theta_{sp}$ and on the proper decay length were changed by 10%. The resulting mass uncertainty is 0.1 MeV/c^2 and $0.2\,\mu$m on $c\tau$.

In total the systematic uncertainties on the mass and on $c\tau$ are estimated to be 14.9 MeV/c^2 and $3.0\,\mu$m, respectively.

7.3.2.6 Conclusion

With the first fb^{-1} of data CMS is expected to measure the $B_{\rm c}$ mass with an uncertainty of $22.0(stat.) \pm 14.9(syst.)$ MeV/c^2 and $c\tau$ with $13.1(stat.) \pm 3.0(syst.)\,\mu$m, corresponding to a lifetime uncertainty of $0.044(fit) \pm 0.010(syst.)$ ps. About 120 $B_c^+ \to J/\psi\pi^+$, with $J/\psi \to \mu^+\mu^-$, events would be observed. At the moment, the theoretical calculation is at the leading order without the colour-octet contribution. Therefore the uncertainties on the total cross section and the $p_{\rm T}$ distribution are large. In the real data analysis, $J/\psi+$ one track with $J/\psi \to \mu^+\mu^-$ will be selected as a control sample, $B^+ \to J/\psi K^+$ will be used to estimate the efficiency, and the side band of the J/ψ peak will be used to estimate the background to $B_{\rm c}$.

7.4 Diffraction and forward physics

7.4.1 Introduction

This section outlines the diffractive and forward physics that CMS can do – together with the TOTEM experiment. The CMS and TOTEM detectors involved are presented in Chapter 7 of Volume 1 of the CMS Physics TDR [7].

The combined phase space coverage of the two experiments makes it possible to study many physics subjects in diffractive interactions – from QCD and the investigation of the low-x structure of the proton to the production of SM and MSSM Higgs bosons. Diffractive events are characterised by the fact that the incoming proton(s) emerge from the interaction intact, or excited into a low mass state, with only a small energy loss. Diffractive processes with proton energy losses up to a few per cent are dominated by the exchange of an object with vacuum quantum numbers, the so called Pomeron, now understood in terms of partons from the proton. For larger energy losses, mesonic exchanges – Reggeons and pions – become important. The topology of diffractive events is characterised by a gap in the rapidity distribution of final-state hadrons due to the lack of colour of the exchanged object.

Events with a fast proton in the final state can also originate from the exchange of a photon. In particular, forward tagging one leading proton allows the selection of photon-proton events with known photon energy; likewise, tagging two leading protons gives access to photon-photon interactions of well known centre-of-mass energy.

Triggering of diffractive/forward events is discussed in [246] and in Appendix E.3. More details on the work presented here can be found in [247].

7.4.2 The interest of diffractive interactions

The study of hard diffraction has been pioneered by the UA8 experiment at CERN [248]. There have been major advances in this field recently, largely driven by the study of diffraction at HERA and the Tevatron. The essential results are discussed in [249] and can be summarised as follows:

- Many aspects of hard diffractive processes are well understood in QCD: the presence of a hard scale allows the use of perturbative techniques and thus to formulate the dynamics in terms of quarks and gluons.
- A key to this success are factorisation theorems in electron-proton scattering, which render part of the dynamics accessible to calculation in perturbation theory. The remaining non-perturbative quantities are the so-called diffractive parton distrib-

ution functions (dPDFs) and generalised (or "skewed") parton distributions (GPDs). They can be extracted from measurements and contain specific information about small-x partons in the proton that can only be obtained in diffractive processes.

Diffractive parton densities are determined from inclusive diffractive processes and can be interpreted as conditional probabilities to find a parton in the proton when the final state of the process contains a fast proton of given four-momentum. Generalised parton distributions can be accessed in exclusive diffractive processes; they quantify correlations between parton momenta in the proton. Their t-dependence is sensitive to the distribution of partons in the transverse plane.

- To describe hard diffractive hadron-hadron collisions is more challenging since factorisation is broken by rescattering between spectator partons. These soft re-interactions can produce additional final-state particles which fill the would-be rapidity gap. When such additional particles are produced, a very fast proton can no longer appear in the final state because of energy conservation. The effect is often quantified in terms of the so called "gap survival probability". These rescattering effects are of interest in their own right because of their intimate relation with multiple scattering effects, which at LHC energies are expected to be crucial for understanding the structure of events in hard collisions.

  The dynamics of rescattering and multi-gap events is still not completely understood. The available data can be described in terms of an effective, non-linear Pomeron trajectory [250]; its variation with energy would be a consequence of multi-Pomeron exchange effects [251]. Other models, also testable at the LHC have been proposed (see e.g. [252] and references therein). These topics can be pursued in more detail with the CMS-TOTEM data at the LHC.
- A fascinating link has emerged between diffraction and the physics of heavy-ion collisions through the concept of saturation, which offers a new window on QCD dynamics in the regime of high parton densities.
- Perhaps unexpectedly, the production of a SM or MSSM Higgs boson in diffractive pp collisions is drawing more and more attention as a clean channel to study the properties of a light Higgs boson or even to discover it. The central exclusive reaction, $pp \to pHp$, appears particularly promising.

7.4.3 A survey of the accessible diffractive/forward processes

The accessible physics is a function of the integrated luminosity. We assume standard LHC optics with $\beta^* = 0.5$ m unless stated otherwise. We recall that, in this case, the TOTEM Roman Pots (RP) at 220 m from the CMS interaction point have coverage for $0.02 < \xi < 0.2$, where ξ is the proton fractional momentum loss. Near-beam detectors at 420 m from the interaction point, currently also being considered [253], would cover $0.002 < \xi < 0.02$.

Low-luminosity ($\sim 10^{28} - 10^{30}\,\mathrm{cm}^{-2}\,\mathrm{s}^{-1}$) studies could profit from running with $\beta^* > 0.5$ m, where the ξ coverage of the 220 m RPs would be wider and the t resolution would improve because of the lower transverse momentum spread of the beam.

7.4.3.1 Inclusive single diffraction and double Pomeron exchange at low luminosity

At modest instantaneous luminosities, up to $10^{32}\,\mathrm{cm}^{-2}\,\mathrm{s}^{-1}$, inclusive single diffractive (SD) events, $pp \to pX$, as well as inclusive double-Pomeron exchange (DPE) events, $pp \to pXp$, can be studied by requiring the presence of one or two rapidity gaps in the event. In the

ξ range given above, the scattered proton can be detected and the kinematics of the events fully measured.

The inclusive SD and DPE cross sections, as well as their M_X dependence, even in the absence of a hard scale, are important quantities to measure at the LHC. Here M_X indicates the mass of the system X. These cross sections amount to approximately 15% and 1% of the total proton-proton cross section, respectively; their energy dependence is a fundamental parameter of (non-perturbative) QCD. In addition, since diffractive events constitute a major fraction of the pile-up events, their measurement is mandatory to be able to properly simulate and understand high-luminosity data, where, at instantaneous luminosities of $10^{34}\,\mathrm{cm}^{-2}\,\mathrm{s}^{-1}$, approximately 35 pile-up events are superimposed, on average, to any event.

7.4.3.2 SD and DPE production of dijets, vector bosons and heavy quarks

The study of SD and DPE events in which the diffractively excited state includes high-E_T jets, heavy quarks or vector bosons opens up the possibility of accessing dPDFs and GPDs. The comparison of the DPE and SD rates for these processes may also give information on the hard diffractive factorisation breaking at LHC (see Sect. 7.4.2). A few examples of these processes are given here.

Production of dijets

The measurement of the reaction $pp \to pXjj$ (j indicates a jet) has been used for the first time by CDF to measure the diffractive structure function in antiproton-proton collisions [254]. A similar measurement is possible at LHC with wider kinematic coverage (CDF: $\xi > 0.035$) and larger minimum jet E_T. For $E_\mathrm{T} > 45\,\mathrm{GeV}$, of the order of 10^8 events per fb^{-1} can be expected.

Production of heavy quarks

Inclusive DPE production of $t\bar{t}$ pairs has been studied in the case in which the final state contains one muon and four jets (i.e. with one top quark decaying to b plus lepton and neutrino, and the other to three jets). The analysis required the detection of both final-state protons. The expected number of events is of order $1 - 100$ for $10\,\mathrm{fb}^{-1}$, depending on the theoretical model assumed.

SD and DPE production of B-mesons has also been looked at, with $B \to J/\psi X$ and $J/\psi \to \mu^+\mu^-$. Here the number of expected events is much larger, of the order of a few events per 10 fb^{-1} in the DPE case and thousands in the SD case.

Inclusive DPE production of W bosons

Inclusive DPE production of W bosons, $pp \to pXWp$, is also sensitive to the dPDFs of the proton and is a relatively abundant process that can be studied at instantaneous luminosities where pile-up is small. In these conditions, the requirement that two final state protons be measured in the 220 m RPs suppresses both the QCD background and the inclusive W production. Several thousand events with $W \to e\nu$ or $W \to \mu\nu$ are expected, after cuts, for an integrated luminosity of $1\,\mathrm{fb}^{-1}$. This process, in conjunction with SD production of W bosons, can be used to study hard diffractive factorisation breaking using the LHC data alone, as mentioned above.

7.4.3.3 SM and MSSM central exclusive Higgs production

As the delivered luminosity reaches tens of fb^{-1}, the central exclusive production process (DPE) becomes a tool to search for new physics, delivering signal to background ratios of order $0.1 - 1$ for Standard Model (SM) Higgs production [255] and more than an order of magnitude larger for certain supersymmetric (MSSM) scenarios.

By central exclusive, we refer to the process $pp \to p\phi p$, where there are large rapidity gaps between the outgoing protons and the decay products of ϕ. There are three primary reasons why this process is attractive. Firstly, if the outgoing protons remain intact and scatter through small angles, then, under some general assumptions, the central system ϕ is produced in the $J_Z = 0$, C and P even state. Secondly, the mass of the central system can be determined very accurately from a measurement of the transverse and longitudinal momentum components of the outgoing protons alone. This means an accurate determination of the mass irrespective of the decay mode of the centrally produced particle. Thirdly, the process delivers excellent signal to background ratios, due to the combination of the J_Z=0 selection rules, the mass resolution, and the simplicity of the event in the central detectors. An additional attractive property of central exclusive production is its sensitivity to CP violating effects in the couplings of the object ϕ to gluons.

The left panel of Fig. 7.14 shows the cross section times the branching ratio for central exclusive production of a Standard Model Higgs, with $H \to b\bar{b}$ and $H \to WW$, as a function of the Higgs mass for different theoretical approaches. The $b\bar{b}$ mode is particularly interesting for masses close to the current exclusion limit. The right panel of Fig. 7.14 shows the acceptance assuming various combinations of RPs at 220 m and near-beam detectors at 420 m. Both protons can be detected in the 220 m stations only for Higgs masses larger than $280\,\text{GeV/c}^2$; this reflects the ξ range for which the 220 m RPs have acceptance, $0.02 < \xi < 0.2$ (the mass of the centrally produced Higgs is related to the ξ via $M_H^2 = \xi_1\xi_2 s$, with ξ_1, ξ_2 the fractional momentum losses of the two protons). However, asymmetric events with one proton at low ξ and another at large ξ can be detected by the combination of the 220 m and 420 m detectors ($0.002 < \xi < 0.02$).

Central exclusive production is generally an attractive way of searching for any new particles that couple strongly to glue. An example studied in [256] is the scenario in which the gluino is the lightest supersymmetric particle. In such models, there should exist a spectrum of gluino-gluino bound states which can be produced in the central exclusive channel. Likewise, central exclusive production of radions, the fields introduced in the Randall-Sundrum model of five-dimensional quantum gravity, has been studied [257].

$H \to b\bar{b}$

The analysis is based on the requirement of two back-to-back central b-tagged jets in addition to the detection of both final-state protons yielding a mass of the central system consistent with that calculated from the protons alone. The event yield is very low, about $2 - 4$ events per $30\,\text{fb}^{-1}$ after all cuts, depending on the model. The non-resonant continuum b-jet background is largely suppressed by the $J_Z = 0$ rule. The residual background, mostly due to dijet production ($gg \to \text{dijets}$) and diffractive $gg \to b\bar{b}$ production, is a function of the mass resolution, which is about 1.6% for the '420+420' combination and 5.6% for the '220+420' combination (for $M_H = 120\,\text{GeV/c}^2$). The number of expected background events is of order 10 for $30\,\text{fb}^{-1}$.

$H \to WW$

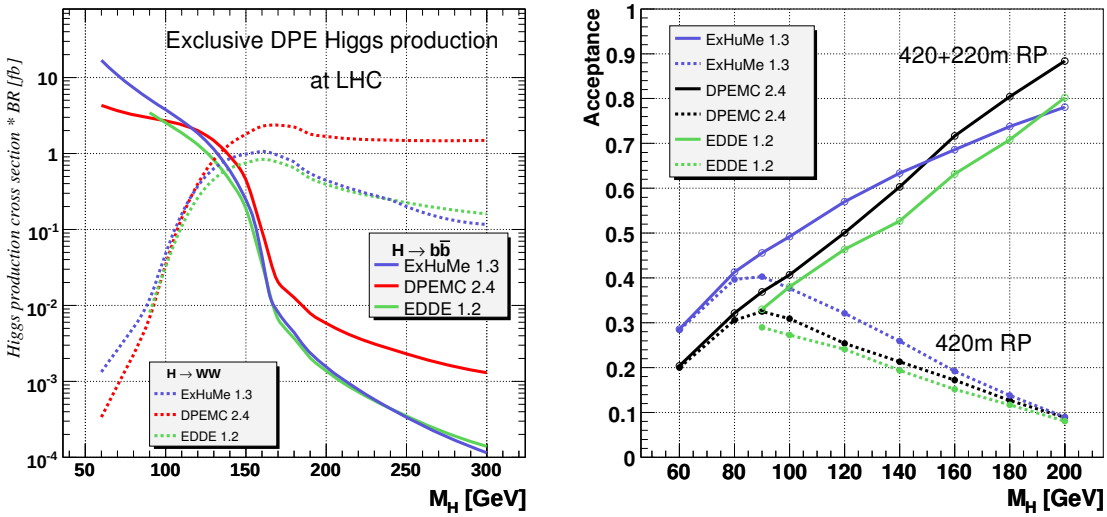

Figure 7.14: Left: The cross section for the exclusive production of the Higgs boson as a function of the Higgs boson mass for $H \to b\bar{b}$ and $H \to WW$. The different curves were obtained with the generators Exhume1.3 [258], DPEMC2.4 [259] and EDDE1.2 [260]. Right: Acceptance for the 420 m detectors alone and for the combination of the 220 m and 420 m detectors as a function of the Higgs boson mass.

In this case, the suppression of the background does not rely primarily on the mass resolution of the RPs. There are three main categories of WW events. Events in which at least one of the W bosons decays to an electron or a muon are the simplest, and pass the Level-1 trigger thanks to the high-p_{T} final-state lepton. This holds also if one of the W bosons decays into a tau, which subsequently decays leptonically. The four-jet mode occurs approximately half of the time; here, however, the RP information is necessary already at Level-1. The expected event yields range between 1 and 7 events for 30 fb^{-1}, depending on the mass. Irreducible backgrounds are small and controllable.

MSSM Higgs

Double proton tagging is especially beneficial in the MSSM case. The b-jet channel is very important in the 'intense coupling regime' of MSSM ($M_h \approx M_A \approx M_H \approx 100\,\mathrm{GeV/c^2}$) [261]: couplings of the Higgs to gg, WW^*, ZZ^* are strongly suppressed, making the discovery challenging by conventional means. Rates for central exclusive production of the two scalar (0^+) MSSM Higgs bosons (h, H) are more than a factor 10 larger than for the SM Higgs. The enhancement for $H \to b\bar{b}$ is by orders of magnitude in the M_h-max scenario for $M_H \approx 180 - 250\,\mathrm{GeV/c^2}$; likewise for $h \to b\bar{b}$ and $h \to \tau\tau$ for $M_h \approx 90 - 130\,\mathrm{GeV/c^2}$ [262]. In the small α_{eff} scenario, $h \to b\bar{b}$ and $h \to \tau\tau$ can be heavily suppressed for large $\tan\beta$ and for $M_h \approx 120\,\mathrm{GeV/c^2}$ [262], whereas $h \to WW$ may be enhanced by up to a factor 4 compared to the SM predictions. Also, the pseudo-scalar (0^-) Higgs boson (A) is practically not produced in the central exclusive channel, yielding a clean separation of the scalar and pseudo-scalar Higgs bosons, impossible in conventional channels. The good missing mass resolution allows to resolve h, H and, if enough statistics is available, measure their widths. This makes central exclusive production a possible discovery channel. Central exclusive production is also interesting in the '3-way mixing' scenario of CP-violating MSSM [263]: here the 3 neutral Higgs bosons are nearly degenerate, mix strongly and have masses close to $120\,\mathrm{GeV/c^2}$.

Central exclusive production, with its good mass resolution via the scattered protons, may allow disentangling the Higgs bosons by studying the production lineshape. Explicit CP-violation in the Higgs sector causes an asymmetry in the azimuthal distributions of tagged protons (via the interference of P-even and P-odd amplitudes) – a measurement unique at the LHC [261, 264].

7.4.3.4 High-energy photon interactions

A significant fraction of events at the LHC involves photon interactions at energies above the electroweak scale [265]. The protons radiating the photon often survive the collision intact and are scattered at angles comparable to the beam angular divergence. Detection of such events at the LHC will open up a new field of high-energy photon physics, which is briefly outlined below. By requiring the detection of one or two forward protons like in diffractive interactions, photon-photon and photon-proton interactions can be selected. The photon fluxes, and the effective luminosities of photon-photon and photon-proton collisions are well known [266, 267]. The average proton energy loss is larger and the proton scattering angle smaller in photon exchanges than for the diffractive case. This can be used to establish relative contributions of these two processes.

Two-photon exclusive production of W and Z boson pairs

The cross section for the production of W pairs via photon-photon interactions, $pp \to ppWW$, is slightly above 100 fb; in almost half of these events both forward protons are produced within the acceptance of the TOTEM RPs. About 100 events per $10\,\text{fb}^{-1}$ with leptonic W decays can be detected in CMS. This allows a precise study of the gauge couplings, in particular of the $\gamma\gamma WW$ coupling. The expected sensitivity to anomalous quartic gauge couplings (QGCs) will surpass the LEP and Tevatron limits by orders of magnitude. A deviation from the Standard Model predictions would also allow a clean detection of anomalous WW production as predicted e.g. by A. White's theory of the supercritical Pomeron [268]. Two-photon production of Z pairs, $pp \to ppZZ$, is not allowed at the SM tree level, but yields similar sensitivities to the anomalous QGCs in this channel.

Two-photon exclusive production of pairs of SUSY particles

The cross sections for production of pairs of charginos, sleptons and charged Higgs bosons via photon-photon fusion at the LHC decrease rapidly with the masses of these particles [269]. This limits the scope of SUSY searches to particle masses below $150 - 200\,\text{GeV/c}^2$. However, the very clean environment of this reaction makes it attractive compared to other production mechanisms; the final state typically consists of two opposite-sign leptons and of missing p_T. The main background is due to the exclusive production of W pairs discussed above.

Two-photon production of doubly charged Higgs bosons (appearing in GUTs) is strongly enhanced, and leads to exclusive final states with two pairs of same-sign leptons.

Two-photon lepton pair production

Exclusive production of lepton pairs – a purely QED process at low $|t|$ – may serve for calibration of the pp luminosity; it may also be used for calibration of the momentum measurement of the scattered proton. Thousands of exclusive muon pairs are expected to be reconstructed in CMS for an integrated luminosity of $1\,\text{fb}^{-1}$. The striking signature of extremely small muon acoplanarity angles of less than about 10 mrad may be exploited already at the trigger level.

Single W and single top photoproduction

The cross section for single W photoproduction, $pp \to pWjX$, reaches almost 100 pb. This process can be therefore studied already at low luminosity. It also provides a means to study rescattering effects [267]. At higher luminosities, studies of high mass Wj states will be possible; for Wj invariant masses above 1 TeV, tens of events are expected to be detected in CMS (and tagged by TOTEM) per $10\,\text{fb}^{-1}$. This will allow to search for, as an example, an anomalous triple gauge coupling γWW. This process is the main background in the search for anomalous photoproduction of single top.

Associated WH and top pair photoproduction

The associated photoproduction of a SM Higgs boson and a W boson has a cross section of about 20 fb for Higgs mass below $180\,\text{GeV/c}^2$. About 50% of the forward protons are tagged by TOTEM, and events with leptonic W decay can be triggered efficiently in CMS. The cross section for photoproduction of top pairs is slightly above 1 pb. Top pair production is the main background for WH production, and in the photoproduction case the signal-to-background ratio for photoproduction of WH pairs is superior to the one in inclusive production.

7.4.3.5 Drell-Yan

The study of forward production of low mass Drell-Yan lepton pairs at the LHC provides a unique opportunity to directly access low-x partons in the proton. In this process, the lepton pair originates from the annihilation of a quark-anti-quark pair whose fractional momenta, x_1 and x_2, are related to the dilepton mass, M, and rapidity, y, through

$$M^2 = sx_1x_2; \qquad x_{1,2} = \frac{M}{\sqrt{s}} \exp^{\pm y}, \tag{7.2}$$

with $\sqrt{s} = 14\,\text{TeV}$, the centre-of-mass energy of the colliding protons. In order to access low x, a large imbalance in fractional momenta is required, boosting the lepton pair to large rapidities.

The CASTOR calorimeter will cover the pseudorapidity range $5.3 < \eta < 6.6$, corresponding to Bjorken-x values down to 10^{-7}. With CASTOR alone, it may be possible to obtain a crude estimate of the dilepton mass. With the additional information provided by the T2 tracker, one can enhance the signal to background ratio by requiring tracks in association to the electromagnetic energy deposits. As T2 will measure both the azimuthal and polar angles of the tracks, a much more accurate measurement of the opening angle (and therefore of the dilepton mass) and a two-dimensional study in M^2 and x will become possible.

7.4.3.6 Validation of cosmic-ray generators

The correct simulation of the interaction of primary cosmic rays in the PeV energy range with the atmosphere is a key tool in the study of cosmic rays. Unfortunately, the available generators differ significantly in their predictions for the energy flow, multiplicity, hadronic energy fraction etc., in particular at high rapidities. These models can be tested at the LHC: a 100 PeV fixed-target collision in air corresponds to the centre-of-mass energy of a pp collision at the LHC. Several generators were used to simulate inelastic and diffractive collisions at CMS: QGSJET [270], SIBYLL [271], DPMJET [272], NEXUS [270]. There are significant differences in the predictions, notably in the region covered by CASTOR, T1 and T2. A measure-

ment of these features with CASTOR, T1 and T2 may thus be used to validate/tune these generators.

7.5 Physics with heavy ions

7.5.1 High-density QCD: heavy-ion physics

Quantum Chromodynamics (QCD) is the only existing quantum field theory within the Standard Model, whose collective behaviour, phase diagram and phase transitions, are accessible to study in the laboratory. High-energy nucleus-nucleus collisions offer the only experimental means known so far to concentrate a significant amount of energy ($\mathcal{O}(10\,\mathrm{TeV})$ at the LHC) in a "large" volume ($\mathcal{O}(100\ \mathrm{fm}^3)$ at thermalisation times of $\tau_0 \approx 1\ \mathrm{fm}/c$), allowing the study the many-body dynamics of strongly interacting matter. The programme of high-energy heavy-ion physics addresses several key open questions of the strong interaction:

- **Deconfinement and chiral symmetry restoration**: Lattice QCD calculations predict a new form of matter at energy densities above $\varepsilon \approx 1\,\mathrm{GeV}/\mathrm{fm}^3$ consisting of an extended volume of deconfined and bare-mass quarks and gluons: the Quark Gluon Plasma (QGP) [273]. The scrutiny of this new state of matter (equation-of-state, order of the phase transition, ...) promises to shed light on fundamental questions such as the nature of confinement, the mechanism of mass generation (chiral symmetry breaking, structure of the QCD vacuum) and hadronisation, that still evade a thorough theoretical description due to their highly non-perturbative nature.
- **Non-linear parton evolution at small-x**: At high energies, hadrons consist of a very dense system of gluons with small (Bjorken) parton fractional momenta $x = p_{parton}/p_{hadron}$. At low-$x$, the probability to emit an extra gluon is large $\sim \alpha_S \ln(1/x)$ and non-linear gluon-gluon fusion processes start to dominate the parton evolution in the hadronic wave functions. Whereas at values of $x \gtrsim 10^{-3}$, the parton evolution with Q^2 (or $\ln(1/x)$) is described by the usual DGLAP (or BFKL) equations, at lower values of x and around $Q_s^2 \sim 3\,\mathrm{GeV}^2/c^2$, such a saturated configuration is theoretically described in terms of the "Colour Glass Condensate" (CGC) picture [274]. Since the nonlinear growth of the gluon density depends on the transverse size of the system, the effects of gluon saturation are expected to set in earlier (at higher x) for heavy nuclei than for free nucleons.

In addition, the study of heavy-ion collisions has interesting connections to other research areas such as:

- **Early Universe cosmology**: The quark-hadron phase transition took place some 10 μs after the Big-Bang and was the most important event taking place in the Universe between the electro-weak (or SUSY) transition ($\tau \sim 10^{-10}$ s) and Big Bang nucleosynthesis (BBN, at $\tau \sim 200$ s). Depending on the order of the QCD phase transition, several cosmological implications such as the formation of strangelets and cold dark-matter (WIMP) clumps or baryon fluctuations leading to inhomogeneous nucleosynthesis, have been postulated [275].
- **High-energy cosmic-ray physics**: The energy and mass of cosmic particles with energies above 10^{14} eV can only be measured via the ground-based detection of "extended air showers" (EAS) generated in upper-atmosphere interactions of cos-

mic rays (protons and ions up to Fe) with air (N,O nuclei). The interpretation of the EAS (and the related astro-particle phenomena) relies heavily on the accurate modelling of hadronic multi-particle production in proton-nucleus (p+N, p+O) and nucleus-nucleus (He+N, N+N, Fe+N) collisions in the TeV range. Direct measurements at LHC are needed in order to calibrate and tune the EAS models and correctly extrapolate their predictions to the highest cosmic-ray energies measured ($\sim 10^{20}$ eV).

- **Gauge/String duality**: Theoretical calculations based on the AdS/CFT correspondence permit to obtain results in strongly coupled ($g^2\,N_c \gg 1$) gauge theories (QCD-like: SUSY $\mathcal{N} = 4$ Yang-Mills) in terms of a dual gravity theory. Recent applications of this formalism have allowed, for the first time, to compute finite temperature QCD transport coefficients (such as the ratio of the QGP viscosity over entropy density, η/s) experimentally accessible, from black hole thermodynamics calculations [276].

7.5.2 Hard probes of QCD matter at LHC

Nucleus-nucleus collisions at the LHC offer a unique opportunity for studying strongly interacting matter at values of energy and particle densities never reached before. The factor of 30 increase in energy between RHIC and the LHC ($\sqrt{s_{NN}}$ = 5.5 TeV for PbPb) leads to copious production of hard QCD probes: high-p_T hadrons, jets, quarkonia, direct photons, etc., arising from parton-parton scatterings with large squared momentum transfer, Q^2. Such perturbative processes take place at time scales $\tau \approx 1/p_{\rm T} \lesssim 0.1$ fm/c, and involve primary partons with fractional momenta of order $x \sim 10^{-3}(10^{-5})$ at central (forward) rapidities. The produced hard probes are, thus, sensitive to initial-state modifications of the low-x parton distribution functions, as well as to final-state effects while propagating through the bulk matter formed in the collision.

The contribution of CMS to the heavy-ion physics programme at LHC is extremely competent based on a number of unique experimental capabilities including:

(i) Very large acceptance at midrapidity ($|\eta| < 2.5$, full ϕ) for layered detection of charged hadrons (with the best momentum resolution for charged tracks at LHC) and neutral hadrons as well as muons, electrons, and photons over a wide range of p_T.

(ii) The best mass resolution of any LHC detector for quarkonia (J/ψ, Υ) measurements leading to clean separation of the various states, improved signal over background, and large reconstructed yields. item (iii) Complete electromagnetic and hadronic calorimetry since day-1 for full jet triggering and reconstruction over $|\eta| < 3$ and $\Delta\phi = 2\pi$ with a large statistical significance for single jet and jet+X channels (X = jet, γ, Z), and for full b- and c- jet identification, allowing detailed studies of "jet quenching" phenomena.

(iv) Unparalleled forward physics (low-x QCD) capabilities thanks to the forward hadronic calorimeter HF (3< $|\eta|$ <5), CASTOR-TOTEM (5.5< $|\eta|$ <6.6), and Zero-Degree-Calorimeter ($|\eta|$ >8.1 for neutrals) detector systems.

(v) A DAQ system capable of delivering almost every PbPb event to the High Level Trigger allowing maximum flexibility to select rare probes at the highest multiplicities expected at the LHC.

Among the various perturbative probes accessible to measurement, we focus on this report on the quarkonia detection via the $\mu^+\mu^-$ decay channel. Other experimental capabilities, in the hard (notably jet reconstruction in the heavy-ion environment), soft (hadron multiplicities, elliptic flow ...), and low-x (e.g. quarkonia photoproduction in electromagnetic PbPb interactions) sectors will be discussed in detail in CMS Physics TDR addendum for Heavy Ions."

7.5.3 Gluon saturation and QGP colour screening via Quarkonia

The production of heavy-quarks at LHC proceeds mainly via gluon-gluon fusion processes and, as such, is sensitive to nuclear modifications of the gluon density at low-x. At $\sqrt{s_{NN}}$ = 5.5 TeV, the average fraction of the nucleon momentum carried by the interacting parton producing a J/ψ at mid (forward) rapidity is $\langle x \rangle \approx 3 \cdot 10^{-3}(10^{-5})$. Such a kinematical domain is well in the regime where gluon saturation effects and departures from linear Q^2 (DGLAP) and $\ln(1/x)$ (BFKL) evolutions should be observable. In addition, the final-state formation of $Q\overline{Q}$ bound states is expected to be suppressed in a deconfined medium due to colour screening of the heavy-quark potential. Recent finite-temperature lattice QCD calculations exhibit a substantial reduction of the heavy-quark internal energy $U_{Q\bar{Q}}$, with increasing temperature. The ground-state charmonium state (J/ψ) has been found to dissolve slightly below $2 \cdot T_{crit} \approx 330$ MeV, whereas much higher dissociation temperatures, $T_{diss} \approx 4 \cdot T_{crit}$ reachable at LHC, are needed to dissociate the Υ. Although J/ψ suppression has been indeed observed in central A+A collisions both at CERN-SPS and RHIC energies, competing mechanisms to colour deconfinement (hadronic co-movers interactions and charm quark recombination) have been proposed to explain the observed cross-sections. At variance with charmonia states, the study of the much heavier bottomonia spectroscopy accessible at LHC is free from the distorting hadronic and coalescence contributions, and is directly sensitive to the temperature conditions of the produced partonic medium.

CMS has focused on the quarkonia detection through their decays to muon pairs. The good muon momentum resolution translates in an Υ mass resolution of $\sigma = 54$ MeV/c^2 (in the central barrel region $|\eta| < 0.8$), the best of all the LHC detectors. This good resolution provides a clean separation between the members of the Υ family with a consequent improvement in the signal to background ratio, even in head-on PbPb collisions with particle multiplicities as large as $N_{ch}/d\eta|_{\eta=0}$ = 5000. The expected signal/background ratios are $S/B \approx 1(5)$, $S/B \approx 0.1(1)$ for J/ψ and Υ respectively in the full ($|\eta| < 0.8$) rapidity range. In the absence of initial- or final-state medium effects, production cross sections of $B_{\mu\mu}\sigma = 50$ mb and 300 μb respectively will be measured in minimum bias PbPb collisions. The expected reconstructed yields for both charmonium and bottomonium resonances after background subtraction, in one-month data taking (with 50% overall efficiency) and nominal PbPb luminosity (0.5 nb^{-1}), are $\mathcal{O}(1.5 \cdot 10^5)$, $\mathcal{O}(2 \cdot 10^4)$ respectively. These statistics will allow detailed quantitative studies of quarkonia production as a function of p_{T}, rapidity and/or centrality. Any departure from the expected "vacuum" cross-sections will provide valuable information on the initial-state modifications of the nuclear parton (especially, gluon) distribution functions, as well as on the thermodynamical state of the produced medium from the predicted "melting" pattern of different quarkonia states due to colour screening.